SUPPLEMENTAL MATERIAL

Figge et al., http://www.jem.org/cgi/content/full/jem.20081160/DC1

Additional information about the mathematics of the statistical and functional modeling approaches.

Statistical model. The experimentally observed speed and turning angle distributions are plotted in Fig. S1. These distributions are derived from B cell tracks in WT mice that have been recorded with the experimental time resolution of $\Delta t_r = 20$ s (1).

It is important to note that analyzing the same cell tracks for various time resolutions, $\Delta t^n_r \equiv n\,\Delta t_r$ with $n = 1, 2, 3, \ldots$, reveals that the impact of Δt^n_r on the turning angle distribution and the speed distribution is quite different. In general, although the speed distribution changes significantly as a function of the underlying time resolution of evaluation, only minor quantitative changes are observed for the turning angle distribution. This can be seen in Fig. S2 (A and B), where we plot the normalized distributions as obtained from averaging over k = 5 time resolutions Δt^n_r with $n = 1, \ldots, k$. In other words, the plotted distributions are the averaged results of cell track analyses with time resolutions ranging from $\Delta t^n_r = 20$ s to $\Delta t^n_r = 100$ s. We observe that the mean value of the relative standard deviation is an order of magnitude larger for the speed distribution (~70%; see also Fig. S2 C for k = 5) than for the turning angle distribution (~6%; see also Fig. S2 D for k = 5). In Fig. S2 (C and D), we plot the mean standard deviation of the speed distribution and turning angle distribution, respectively, for averages greater than $n = 1$ to k (with k ranging from 1 to 8) involving time resolutions $\Delta t^n_r = 20$ s up to $\Delta t^n_r = 160$ s. It is observed that although the mean standard deviation of the speed distribution is an increasing function of k, for the turning angle distribution, this quantity stays fairly constant at ~6% over the entire range of k values.

Collectively, this analysis shows that, in contrast to the speed distribution, the turning angle distribution is quite robust against variations in the time resolution Δt^n_r of the cell track analysis. We make use of this robustness property in the statistical model by using the turning angle distribution in Fig. S1 B, which has been evaluated with a time resolution of $\Delta t^n_r = 20$ s, at larger time resolutions, which correspond to the directional persistence time Δt_p. The value of $\Delta t_p = 1.24$ min ($\Delta t_p = 1.05$ min) for B cells in WT mice (CXCL13 KO mice) is well within the range of time resolutions for which the turning angle distribution represents a reasonable approximation. Typical variations in the speed and turning angle of a B cell in WT mice during 30 min of cell tracking within the statistical model are plotted in Fig. S3.

The B cell migration between the dark zone and the light zone as measured by the inter-zone migration frequency is plotted in Fig. S4 as a function of the number of zonal transitions. It is generally observed that this frequency is an exponentially decreasing function of the number of zonal transitions for each individual cell and for various minimal migration ranges rmin. The minimal migration range corresponds to the thickness of the zone boundary and sets a lower limit of the distance B cells have to migrate to traverse the zone boundary. For increasing r_{min}, cell wiggling becomes suppressed, which is initially accompanied by an increase of the migration frequency at small zonal transition numbers for a fairly constant total number of zonal transitions. For a simulation time of half an hour (1 h), we observe from Fig. S4 A that this is the case for minimal migration ranges $r_{min} \leq 25$ μm ($r_{min} \leq 40$ μm). Increasing r_{min} further reduces the total number of zonal transitions and ultimately allows only for unidirectional migration events between the dark zone and the light zone (see also Fig. 2 B).

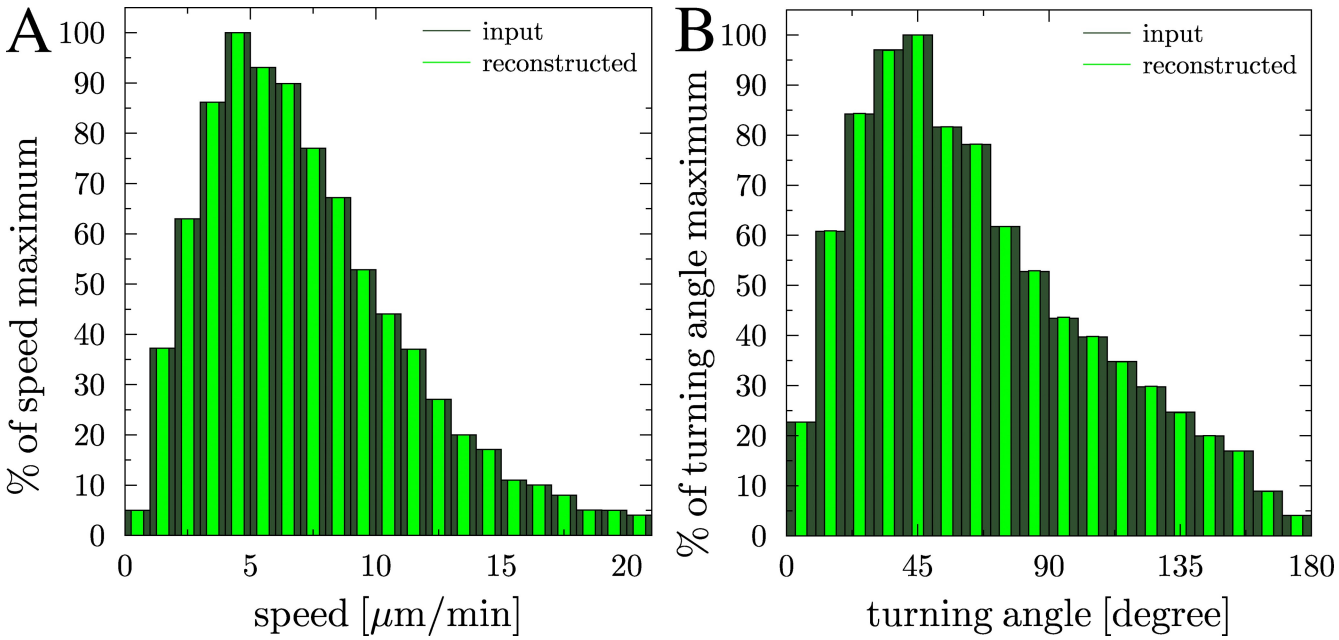

Figure S1. WT B cell speed and turning angle distributions. The speed distribution (A) and turning angle distribution (B) of WT B cells as obtained by Allen et al. (Allen, C., T. Okada, H. L. Tang, and J. Cyster. 2007. *Science*. 315:528–531; dark green) are used as input for the statistical model. Reconstructions of these distributions from the B cell tracks of the statistical model are shown for comparison after 10 min of simulation time (light green).

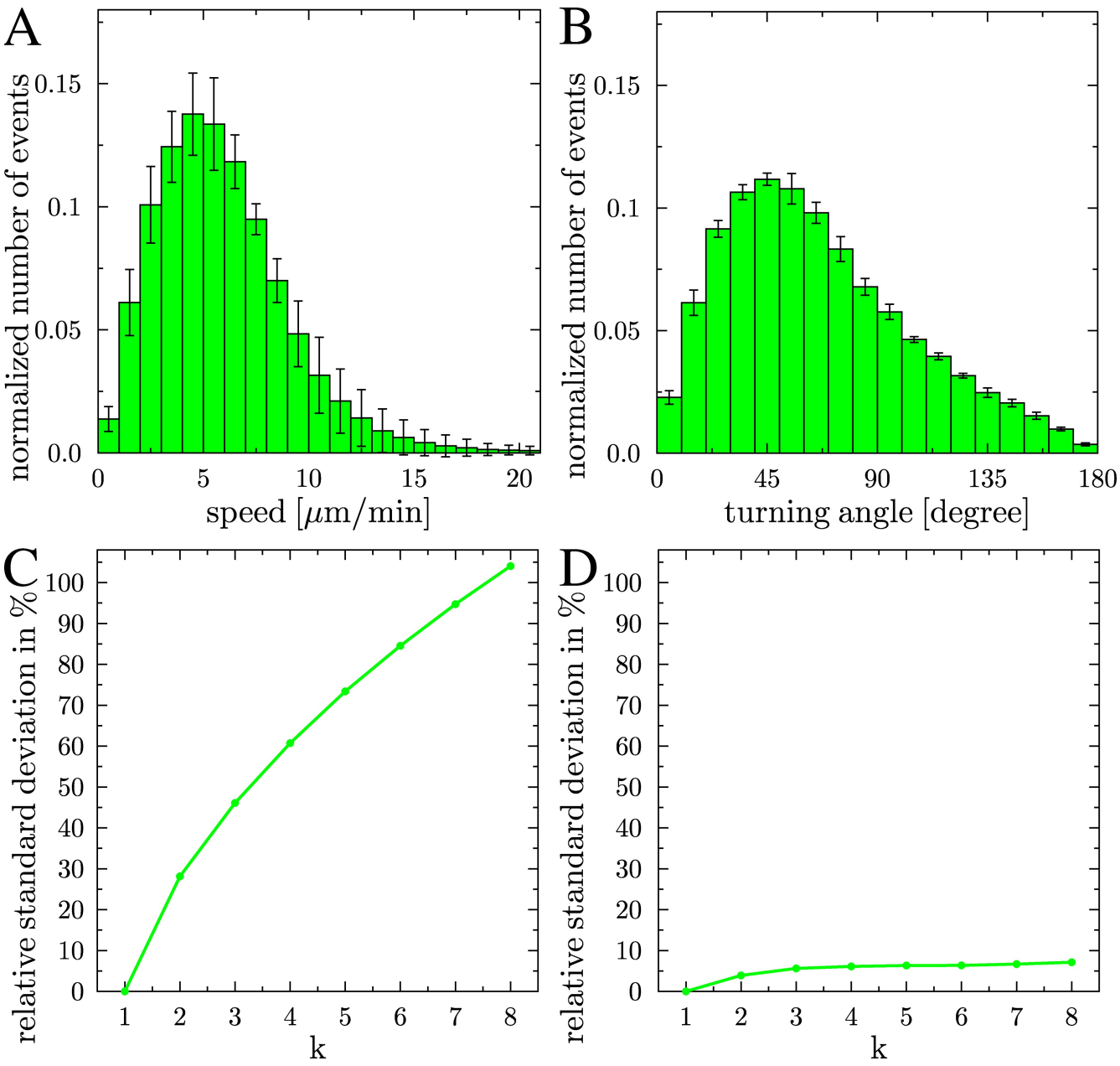

Figure S2. Normalized speed and turning angle distributions as obtained from averaging over different time resolutions. (A) The speed distribution changes with a mean relative SD of ∼70%. (B) The turning angle distribution is robust with a mean relative SD of ∼6%. (C) The mean relative standard deviation for the speed distribution is an increasing function of the total number included time resolutions k. (D) The mean relative standard deviation for the turning angle distribution as a function of k shows its robustness with respect to the time resolution of the cell track evaluation.

Functional model. We developed a hybrid agent-based model for simulations of the GC reaction in three spatial dimensions that relies on previous mathematical models for the GC reaction (2–5). The model consists of three coupled levels. The first level contains the main lattice corresponding to the physical space with lattice constant $\Delta x = 5$ μm, in which cells can migrate and interact. Each biological cell is represented at a single node and evolves according to reaction rates that define a probability of action or interaction with neighboring cells or solubles that are explained in the following paragraph. The time step of $\Delta t = 0.002$ h is smaller than the fastest process of the dynamic system.The second level refers to the shape space (6), which is represented by a four-dimensional lattice encoding the antibody type of each B cell. Somatic hypermutation is represented by switching the antibody type to a neighboring point in the shape space. Without loss of generality, the optimal clone for a given antigen is in the center of the shape space. The Hamming distance of a clone Φ from the optimal clone $\Phi^\star$ is mapped to a quantity $a(\Phi, \Phi^\star)$ associated with the antibody–antigen affinity by the followong (2, 7):

$$a(\Phi,\Phi^\star) = \exp\left(-\frac{|\,|\,\Phi - \Phi^\star\,|\,|_1^2}{\Gamma^2}\right), \quad (1)$$

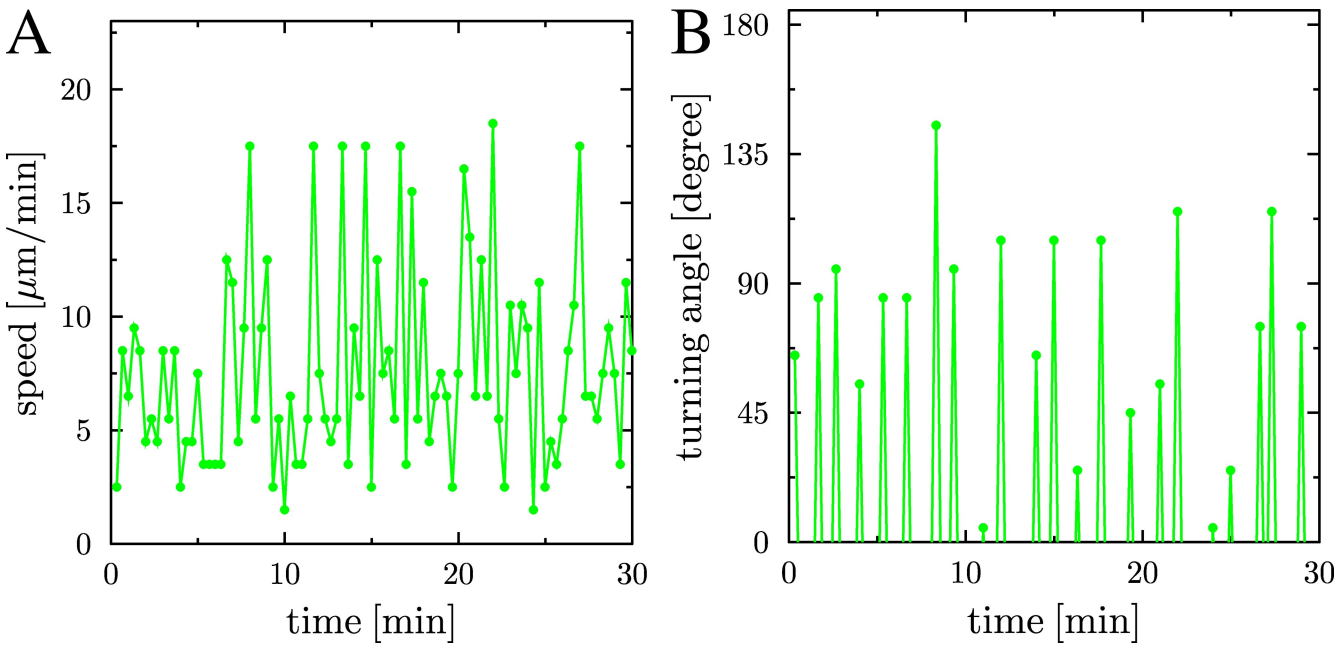

Figure S3. Time-dependent speed and turning angle of a B cell within the statistical model. Typical variations in the speed with time step Δt_v = 20 s (A) and in the turning angle with Δt_p = 1.24 min (B) for B cells in WT mice during half an hour of cell tracking.

where Γ determines the width of the affinity function. This affinity determines the binding probability of a cell object to an FDC. The third level deals with solving a system of reaction-diffusion equations for the solubles. An Alternating-Direction-Implicit (ADI) method is applied to solve the partial differential equations on a lattice. The solubles considered in the following are the chemokines CXCL12 and CXCL13. It is assumed that the sources for CXCL12 are stromal cells at the border of the follicle to the T zone, and the FDCs in the light zone for CXCL13.

The considered reactions are listed as follows (please refer to Table S1 for parameter values): (a) monoclonal expansion of centroblasts in the FDC network lasts for 3 d with 6 h cycle time (8). The simulation starts at day one with 60 seeder cells derived from 5 seeder clones. All seeder clones have a distance of five mutations from the clone with optimal affinity. The 60 cells are randomly distributed in the GC volume. (b) Centroblast proliferation is modeled by occupation

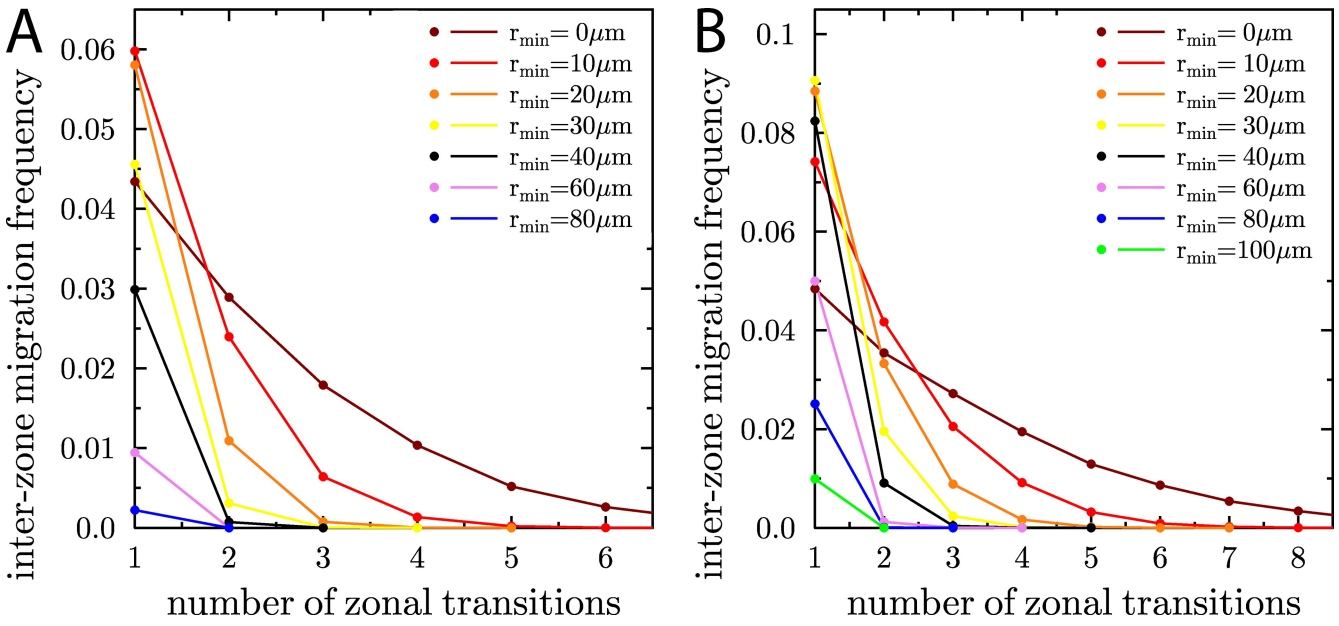

Figure S4. B cell migration between the dark zone and the light zone in the statistical model. (A) Inter-zone migration frequency for B cells in WT mice as a function of the number of zonal transitions for each individual cell across the zone boundary at plane intercept 0 μm and for different minimal migration ranges r_{min} across the zone boundary. The simulation time is half an hour. (B) The same as before for 1 h simulation time.

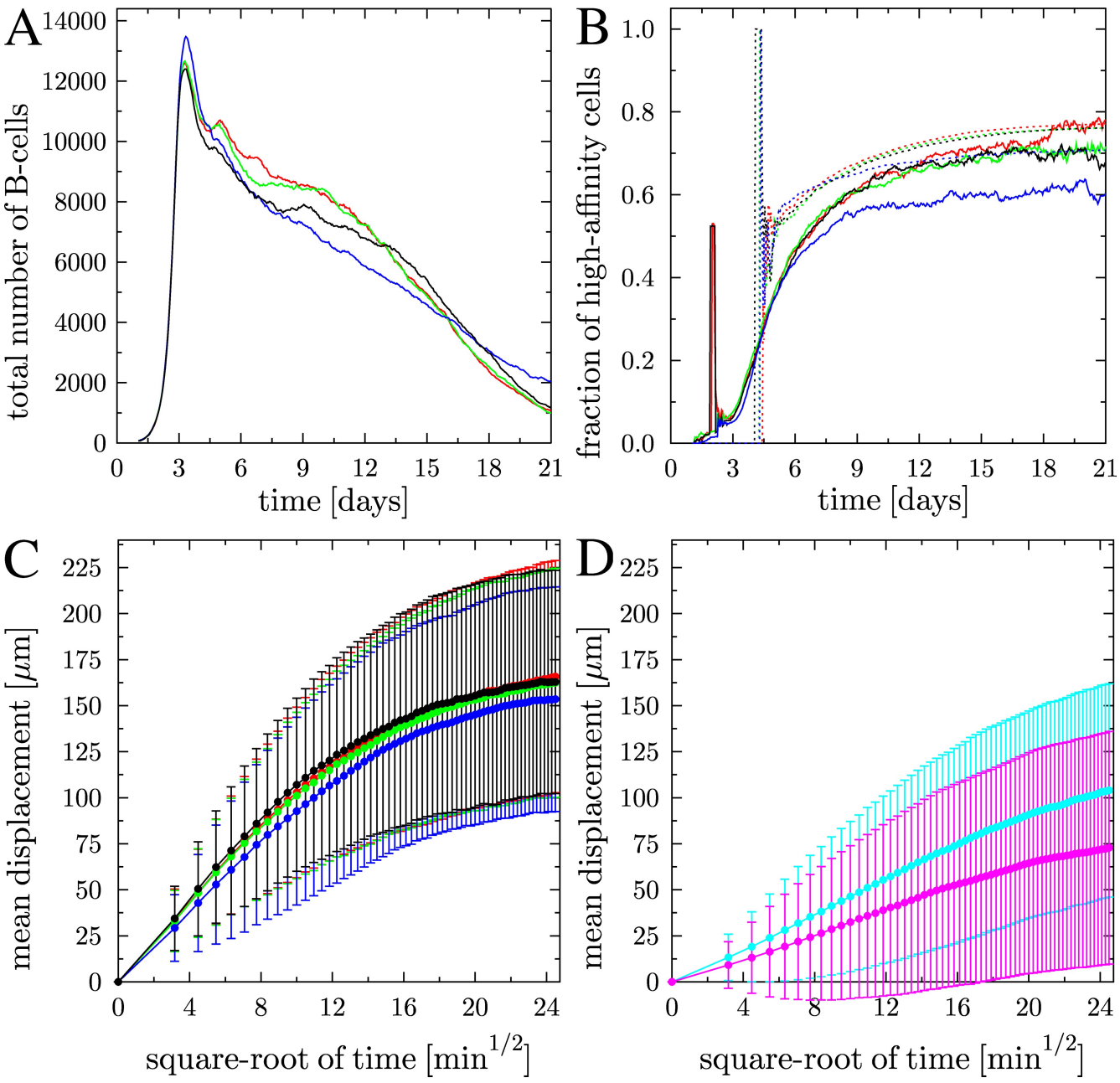

Figure S5. Analysis of the GC reaction in the functional models. The population kinetics (A), affinity maturation (B), and mean displacement curves (C) during the GC reaction for the random migration model (red), the transient model with weak (green) and moderate (blue) chemotaxis, and the desensitization model with moderate chemotaxis (black). Both B cells (B, solid lines) and accumulated output cells (B, dotted lines) are shown. The results are comparable with each other, even though the corresponding GC morphologies are quite different (Fig. 5). In the absence of desensitization mechanisms, the observed mean displacement is significantly reduced (D). This is shown for moderate (cyan) and strong (magenta) chemotaxis.

of a neighboring node (Moore neighborhood). If all Moore neighbors are occupied, cell division is suppressed. (c) Somatic hypermutation is induced with a mutation probability of 0.5 in each division (9). Mutations are represented by jumps in the aforementioned four-dimensional shape space to the nearest neighbor points. (d) From day three after onset of proliferation, differentiation of centroblasts into centrocytes is initiated with an inverse rate of 4 h. To guarantee similar population kinetics (Fig. S5 A), the inverse rate is increased to 4.5 h in the case of the transient model with moderate chemotaxis strength. Differentiation is smoothly switched on after a sigmoidal function with a width of 3 h at approximately t = 69 h. (e) The preformed FDC network consists of 200 FDCs that are distributed randomly within two-thirds of the maximum GC volume. (f) Interaction with FDCs is mediated by presented antigen portions. One such portion corresponds to the number of molecules sufficient to induce signaling in the B cell. A finite amount of such portions is distributed on the dendrites of each FDC at the beginning of the simulation. Each FDC has six dendrites of 40 μm length. The nodes associated with the dendrites can still be occupied by B cells. Antigen on the dendrites can be accessed by B cells from the site itself and from all nearest-neighbor sites. (g) Centrocytes are rescued from apoptosis

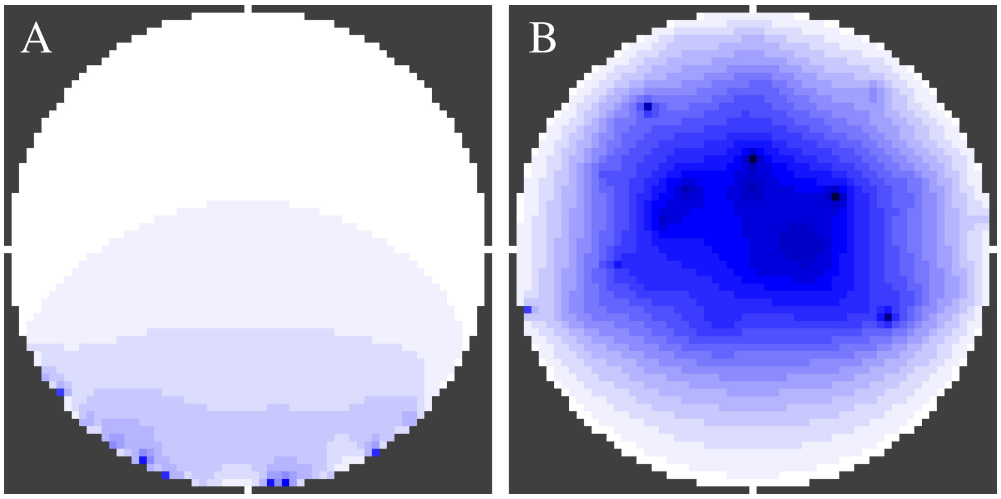

Figure S6. GC chemokine distribution of CXCL12 and CXCL13 in the functional model. B cells are sensitive to the gradient of the chemokine CXCL12 released by stromal cells at the border of the follicle toward the T zone (A) and of the chemokine CXCL13 released by FDCs in the light zone (B). In the simulations, B cells are optionally desensitized by sufficiently high values of the chemokine concentrations nearby the sources. The amount of chemokine is proportional to the color intensity (arbitrary units).

by interaction with antigen presented on FDC. The binding probability depends on the antibody affinity to the antigen. In the model, affinity is described by the Gauss function eq. (1) in the shape space centered at the clone of highest affinity. If antigen is accessible from the node occupied by a centrocyte, the binding probability is given by this Gauss function. (h) We account for antigen consumption by modeling the uptake of antigen by B cells. Above a threshold of 20 antigen portions (at each FDC site), the binding probability is solely determined by the antibody–antigen affinity. Below that threshold, it is linearly decreasing down to zero when the antigen is fully consumed. (i) The survival signal for centrocytes is assumed to be provided within 30 min. In the model, centrocytes are immobile during this period. (j) Centrocytes die by apoptosis in ~10 h (10) and are quickly internalized by phagocytosis. This is modeled by removal of unselected centrocytes from the cell lattice with an inverse rate of 10 h. (k) Re-testing of centrocytes is assumed to remain possible during their lifetime. However, two attempts to bind antigen are assumed to be separated by a refractory time of 12 min (5). (l) FDC-selected centrocytes have to find T cell help for final selection and further differentiation signals. The number of T cells in the GC is fixed to 1,500, which roughly corresponds to 10% of the peak cell population (11). If modeled centrocytes find a T cell on a neighboring site, the interaction is assumed to last for 36 min. (m) Experiments reveal that T helper cells interacting with different B cells polarize toward the B cell with strongest stimulus (12). In the model, T cells polarize their signaling apparatus toward the B cell in contact with highest affinity of the presented antibody. Only if the T cell remains polarized to a B cell for half an hour is the B cell selected, after which it receives further differentiation signals. The apoptotic state is attributed to all other B cells, which may correspond to induction of Fas-mediated apoptosis. Apoptotic cells are quickly removed from the lattice, corresponding to fast phagocytosis. Such an affinity-dependent T cell help was previously hypothesized (5) and is meanwhile supported by experimental findings (13). (n) Positively selected B cells are assumed to get different T cell signals: a probabilistic decision is taken whether the centrocytes differentiate to plasma cells, memory cells, or recycle to proliferating and mutating centroblasts. The latter back-differentiation is assumed to take 5 h. The recycling probability of positively selected centrocytes is set to 1 between day 3 and 5, and to 0.8 from day 5 after onset of proliferation (2), implying a delayed production of plasma cells and memory cells. The transition of the output probability is smoothly controled by a sigmoidal function with a width of 3 h centered at approximately t = 120 h.

Cell motility and chemotaxis. The mean speed of B cells and T cells is assumed to be 8 μm/min and 10 μm/min as observed in vitro, respectively. This induces a reduced average speed in dense tissue, which is in agreement with intravital two-photon imaging data on GC of mice (1, 14, 15). These velocities define displacement probabilities to nearest-neighbor nodes (von Neumann neighborhood). If the target nodes are occupied, the movement is suppressed (with exceptions; see next paragraph).

The preferred direction of movement is defined by a polarity vector that is attributed to each cell. If two neighboring cells exhibit a negative scalar product of their polarity vectors, the two cells exchange sites with a probability of 0.5. In this way, we model that B cells can pass each other even in overcrowded regions of the GC. This procedure removes artifacts in the simulations that might otherwise appear because of the underlying rigid lattice.

The polarity vector is renewed after an average time of 1.24 min for B cells and 1.7 min for T cells, which is associated with the cell persistence time (1, 16). The new polarity vector $\mathbf{p}$ is determined at random and by the influence of chemokine gradients according to the eqaution

$$\mathbf{p} = \mathbf{p}_{rand} + \frac{\alpha}{1 + \exp\left\{\kappa(K_{1/2} - \Delta x \,|\, \nabla c \,|)\right\}} \frac{\nabla c}{|\nabla c|}, \quad (2)$$

where $\mathbf{p}_{\text{rand}}$ is a random polarity vector and α denotes the maximal relative weight of the response to the gradient of the chemokine field c. $K_{1/2}$ is the gradient of half-maximal chemokine weight and κ determines the steepness of its dependence on the chemokine gradient. The random part of the new polarity vector is chosen from a turning angle distribution as measured in two-photon experiment (Fig. S1 B) (1). $\mathbf{p}$ is used as a normalized vector.

CXCL13 is secreted by FDC while CXCL12 is secreted by stromal cells at the border of the follicle toward the T zone. The secretion rate is chosen to get relevant chemokine gradients, as shown in Fig. S6. The steady-state solution of the diffusion equation for both chemokines and Dirichlet boundary conditions with value zero is used.

Three chemotaxis models are considered in the simulations. The first is the random model B cells, which are are insensitive to both chemokines performing pure random walk migration with a directional persistence time of 1.24 min. The second is the transient model. In addition to random walk, migration centrocytes are sensitive to CXCL13 right after differentiation from centroblasts, and proliferating B cells are sensitive to CXCL12 right after accomplished recycling (reacquisition of proliferation potential). The relation of random walk migration and chemotaxis is regulated according to eq. (2). B cells downregulate their sensitivity to chemokines after 6 h. The third is the desensitization model. This is an extension of the transient model, where B cells downregulate their sensitivity to the chemokines after 6 h or in response to an absolute overcritical concentration of these chemokines. The threshold for desensitization is set to typical values as found at a 25-μm distance from the chemokine sources. Desensitized cells remain insensitive to CXCL13 (CXCL12) until further differentiation to centroblasts (centrocytes).

Note that the relative strength of the chemotaxis response can be varied in the transient model and in the desensitization model because the randomly chosen cell polarity is complemented by the chemokine gradient with a tunable weight. Three levels are distinguished in the model: weak chemotaxis ($\alpha = 1$ in eq. [2]) induces only a weak bias toward the chemokine sources of ~10%; moderate chemotaxis ($\alpha = 10$ in eq. [2]) induces an equilibrated choice between randomness and chemokine gradient at ~50%; and strong chemotaxis ($\alpha = 100$ in eq. [2]) determines the new polarity dominantly toward the chemokine gradient well above 50%.

REFERENCES

1. Allen, C.D., T. Okada, H.L. Tang, and J. Cyster. 2007. Imaging of germinal center selection events during affinity maturation. *Science*. 315:528–531.
2. Meyer-Hermann, M.E., A. Deutsch, and M. Or-Guil. 2001. Recycling probability and dynamical properties of germinal center reactions. *J. Theor. Biol.* 210:265–285.
3. Meyer-Hermann, M. 2002. A mathematical model for the germinal center morphology and affinity maturation. *J. Theor. Biol.* 216:273–300.
4. Meyer-Hermann, M.E., and P. Maini. 2005. Back to one-way germinal centers. *J. Immunol.* 174:2489–2493.
5. Meyer-Hermann, M.E., P.K. Maini, and D. Iber. 2006. An analysis of B cell selection mechanisms in germinal centers. *Math. Med. Biol.* 23:255–277.
6. Perelson, A.S., and G.F. Oster. 1979. Theoretical studies of clonal selection: minimal antibody repertoire size and reliability of self-non-self discrimination. *J. Theor. Biol.* 81:645–670.
7. Meyer-Hermann, M.E., and T. Beyer. 2004. The type of seeder cells determines the efficiency of germinal center reactions. *Bull. Math. Biol.* 66:125–141.
8. Hanna, M.G. 1964. An autoradiographic study of the germinal center in spleen white pulp during early intervals of the immune response. *Lab. Invest.* 13:95–104.
9. Berek, C., and C. Milstein. 1987. Mutation drift and repertoire shift in the maturation of the immune response. *Immunol. Rev.* 96:23–41.
10. Liu, Y.J., C. Barthelemy, O. De Bouteiller, and J. Banchereau. 1994. The differences in survival and phenotype between centroblasts and centrocytes. *Adv. Exp. Med. Biol.* 355:213–218.
11. Kelsoe, G. 1996. The germinal center: a crucible for lymphocyte selection. *Semin. Immunol.* 8:179–184.
12. Depoil, D., R. Zaru, M. Guiraud, A. Chauveau, J. Harriague, G. Bismuth, C. Utzny, S. Muller, and S. Valitutti. 2005. Immunological synapses are versatile structures enabling selective T cell polarization. *Immunity*. 22:185–194.
13. Allen, C.D., T. Okada, and J. Cyster. 2007. Germinal-center organization and cellular dynamics. *Immunity*. 27:190–202.
14. Schwickert, T.A., R. Lindquist, G. Shakhar, G. Livshits, D. Skokos, M. Kosco-Vilbois, M. Dustin, and M. Nussenzweig. 2007. In vivo germinal center imaging reveals a dynamic open structure. *Nature*. 446:83–87.
15. Hauser, A.E., T. Junt, T. Mempel, M. Sneddon, S. Kleinstein, S. Henrickson, U. von Andrian, M. Shlomchik, and A. Haberman. 2007. Definition of germinal-center B cell migration in vivo reveals predominant intrazonal circulation patterns. *Immunity*. 26:655–667.
16. Miller, M.J., S. Wei, I. Parker, and M. Cahalan. 2002. Two-photon imaging of lymphocyte motility and antigen response in intact lymph node. *Science*. 296:1869–1873.

Table S1. Parameter table of the functional model

Parameter	Value	Type	Ref.
Lattice constant Δx	5 μm	fixed	
Lattice dimension	3	experiment	
Radius of reaction volume	160 μm	experiment	
FDC network volume per GC volume	2/3	estimated	
Shape space dimension	4	fixed	1, 2
Width of Gaussian affinity weight function Γ	2.8	experiment	3
Time step Δt	0.002 h	fixed	
Duration of optimization phase	51 h	experiment	4, 5, 6
Width of sigmoidal for switch	3 h	fixed	
Number of seeder clones	5	experiment	7–10
Cell cycle time of CB	6 h	experiment	8
Mutation probability of CB	0.5	experiment	11, 12
Duration of CB differentiation to CC	4 h	varied	8, 13
Duration of static FDC-CC contact	30 min	experiment	14
CC refractory time	12 min	fixed	15
Duration of differentiation of selected CC	5 h	estimated	4
Probability of recycling for selected CC	0.8	experiment	3, 16
CC lifetime	10 h	experiment	17
Rate of phagocytosis of apoptotic cells	0.01 h	estimated	
Number of FDCs	200	estimated	
Length of FDC dendrites	40 μm	estimated	15
Number of antigen portions per FDC	1,000	estimated	15
Antigen threshold for maximum binding probability	20	fixed	15
Number of TC	1,500	experiment	18
Duration of CC–TC interaction before apoptosis	36 min	fixed	15
Duration of CC–TC interaction before selection	30 min	fixed	15
Weight of chemotaxis α	1	varied	
Gradient of half-maximal chemotaxis weight K1/2	0.2 nM	fixed	
Steepness of chemotaxis weight κ	10 nM^{-1}	fixed	
CXCL12/13 diffusion constant	10^3 $\mu m^2/h$	fixed	
CXCL13 production rate per FDC	10 nM/h	estimated	
Number of stromal cells	300	estimated	
CXCL12 production rate per stromal cell	400 nM/h	estimated	
Critical CXCL12 concentration for desensitization	0.7 nM	estimated	
Critical CXCL13 concentration for desensitization	0.09 nM	estimated	
Duration of CXCR4/5 expression	6 hr	fixed	
BC speed in vitro	8 μm/min	experiment	19, 20
BC persistence time	1.24 min	experiment	19
TC speed in vitro	10 μm/min	experiment	19, 20
TC persistence time	1.7 min	experiment	19, 21

All parameters and their assumed values as used in the functional model are listed. A category is attributed to each parameter. A fixed parameter is either a purely theoretical parameter or a hypothetical parameter with an assumed value exhibiting robustness against variation. Estimated parameters were obtained from experimental constraints on a phenomenological level. Experiment is attributed to parameter values with direct experimental evidence. Varied parameters were changed for some simulations and are further discussed in the text. The value given here corresponds to the transient weak chemotaxis model. Symbols are given just in the case these are used in the text. TC, T cell; BC, B cell; CB, centroblast; CC, centrocyte; FDC, follicular dendritic cell.

REFERENCES

1. Perelson, A. S., and G. F. Oster. 1979. Theoretical studies of clonal selection: minimal antibody repertoire size and reliability of self-non-self discrimination. *J. Theor. Biol.* 81:645–670.
2. Lapedes, A., and R. Farber. 2001. The geometry of shape space: application to influenza. *J. Theor. Biol.* 212:57–69.
3. Meyer-Hermann, M., A. Deutsch, and M. Or-Guil. 2001. Recycling probability and dynamical properties of germinal center reactions. *J. Theor. Biol.* 210:265–285.
4. Meyer-Hermann, M. 2002. A mathematical model for the germinal center morphology and affinity maturation. *J. Theor. Biol.* 216:273–300.
5. Jacob, J., J. Przylepa, C.Miller, and G. Kelsoe. 1993. In situ studies of the primary response to (4-hydroxy-3-nitrophenyl)acetyl. III. The kinetics of V region mutation and selection in germinal center B cells. *J. Exp. Med.* 178:1293–1307.

6. Pascual, V., S. Cha, M. E. Gershwin, J. D. Capra, and P. S. C. Leung. 1994. Nucleotide sequence analysis of natural and combinatorial anti-pdc-e2 antibodies in patients with primary biliary cirrhosis. *J. Immunol.* 152:2577–2585.
7. Kroese, F. G., A. S. Wubbena, H. G. Seijen, and P. Nieuwenhuis. 1987. Germinal centers develop oligoclonally. *Eur. J. Immunol.* 17:1069–1072.
8. Liu, Y. J., J. Zhang, P. J. Lane, E. Y. Chan, and I. C. M. MacLennan. 1991. Sites of specific B cell activation in primary and secondary responses to T cell-dependent and T cell-independent antigens. *Eur. J. Immunol.* 21:2951–2962.
9. Jacob, J., R. Kassir, and G. Kelsoe. 1991. In situ studies of the primary immune response to (4-hydroxy-3-nitrophenyl)acetyl. I. The architecture and dynamics of responding cell populations. *J. Exp. Med.* 173:1165–1175.
10. Küppers, R., M. Zhao, M. L. Hansmann, and K. Rajewsky. 1993. Tracing B cell development in human germinal centers by molecular analysis of single cells picked from histological sections. *EMBO J.* 12:4955–4967.
11. Berek, C., and C. Milstein. 1987. Mutation drift and repertoire shift in the maturation of the immune response. *Immunol. Rev.* 96:23–41.
12. Nossal, G. J. 1992. The molecular and cellular basis of affinity maturation in the antibody response. *Cell.* 68:1–2.
13. Meyer-Hermann, M. 2002. Does recycling in germinal centers exist? *Immunol. Cell Biol.* 80:30–35.
14. van Eijk, M., J. P. Medema, and C. de Groot. 2001. Cellular Fas-associated death domainlike IL-1-converting enzyme-inhibitory protein protects germinal center B cells from apoptosis during germinal center reactions. *J. Immunol.* 166:6473–6476.
15. Meyer-Hermann, M., P. K. Maini, and D. Iber. 2006. An analysis of B cell selection mechanisms in germinal centers. *Math. Med. Biol.* 23:255–277.
16. Han, S. H., B. Zheng, J. Dal Porto, and G. Kelsoe. 1995. In situ Studies of the Primary Immune Response to (4-Hydroxy-3-Nitrophenyl) Acetyl IV. Affinity-dependent, antigen-driven B-cell apoptosis in germinal centers as a mechanism for maintaining self-tolerance. *J. Exp. Med.* 182:1635–1644.
17. Liu, Y. J., C. Barthelemy, O. De Bouteiller, and J. Banchereau. 1994. The differences in survival and phenotype between centroblasts and centrocytes. *Adv. Exp. Med. Biol.* 355:213–218.
18. Kelsoe, G. 1996. The germinal center: a crucible for lymphocyte selection. *Semin. Immunol.* 8:179–184.
19. Miller, M., S. Wei, I. Parker, and M. Cahalan. 2002. Two-photon imaging of lymphocyte motility and antigen response in intact lymph node. *Science.* 296:1869–1873.
20. Wei, S. H., I. Parker, M. J. Miller, and M. D. Cahalan. 2003. A stochastic view of lymphocyte motility and trafficking within the lymph node. *Immunol. Rev.* 195:136–159.
21. Meyer-Hermann, M., and P. Maini. 2005. Interpreting two-photon imaging data of lymphocyte motility. *Physical Review E.* 71:061912.